Fluid-induced fault reactivation due to brucite + antigorite dehydration triggered the Mw7.1 September 19th Puebla-Morelos (Mexico) intermediate-depth earthquake

F. Gutiérrez-Aguilar[1], D. Hernández-Uribe[2,3*], R. M. Holder[3], and C. B. Condit[4]

[1]*Facultad de Ingeniería, Universidad Nacional Autónoma de México, Ciudad de México 04510, México*

[2]*Department of Earth and Environmental Sciences, University of Illinois, Chicago, Illinois 60607 U.S.A.*

[3]*Department of Earth and Environmental Sciences, University of Michigan, Michigan 48109, U.S.A.*

[4]*Earth and Space Sciences Department, University of Washington, Washington 98105, U.S.A.*

*Corresponding author: D. Hernández-Uribe (dav.hernandez.uribe@gmail.com)

Key Points:

- The dehydration of antigorite + brucite has a positive total volume change and leads to fluid-induced fault reactivation.
- We hypothesize that fluid-induced fault reactivation triggered the Puebla-Morelos 2017 earthquake.
- The antigorite + brucite reaction only happens in highly hydrated regions of the upper lithospheric mantle.

Abstract

The Puebla-Morelos (Mexico) 2017 earthquake nucleated ~250 km inland from the trench within the Cocos oceanic plate mantle. Here, we argue that the Puebla-Morelos (Mexico) 2017 earthquake resulted from changes in effective stress due to the reaction brucite + antigorite = olivine + H_2O leading to the reactivation of pre-existing seafloor faults. Fluid release (~185 kg of H_2O per m^3 of subducted hydrated harzburgite) and volume increase ($\Delta Vr_{\text{solid + fluid}}$ = ~0.8%) likely occur along subducted seafloor-inherited faults. The amount of H_2O released, and magnitude of volume change depends on the degree of faults hydration; only highly hydrated (> 40 % of hydration) faults will stabilize brucite and experience this reaction at depth. The brucite + antigorite dehydration reaction may be key for intermediate seismicity worldwide.

Plain Language Summary

The Puebla-Morelos (central Mexico) Mw7.1 earthquake occurred in an uncommon locality in Mexico compared to most of the catastrophic earthquakes that have occured in this part of the world—it nucleated ~250 km inland, almost below Mexico City. In this paper, we explore the role of mineralogical changes occurring in the Cocos tectonic plate, which is currently descending below the North America plate. Our model tracked the changes in the minerals within the rocks and show that the earthquake might have been triggered by the physical changes associated with the mineral reaction: brucite + antigorite = olivine + H_2O. We suggest that this mineral reaction primarily occurred along faults in the subducting oceanic floor along which the mantle lithosphere was hydrated prior to subduction. The brucite + antigorite dehydration reaction may be key for intermediate seismicity worldwide.

1. Introduction

The young oceanic Cocos plate (<20 Myr; Müller et al., 2008), in western Mexico, subducts underneath North America's continental lithosphere at an angle of ~15° at the Guerrero trench (Pérez-Campos et al., 2008). Inland ~125 km, subduction becomes near-horizontal for 150 km, before steepening to ~75° and extending to ~550 km depth (Pérez-Campos et al., 2008). Historically, earthquakes in Mexico occur along the Pacific coast megathrust (Fig. 1), including the devastating September 19th 1985 Mw8.5 Michoacán earthquake. The September 19th 2017 Mw7.1 Puebla-Morelos earthquake is considered atypical due to its location as it nucleated inland (~250 km from the trench; Fig.1) near the end of the Cocos flat slab segment where the subduction dip angle steepens, with a hypocenter located at ~57 km depth, within the Cocos lithospheric mantle (Servicio Sismológico Nacional—SSN, 2020). This earthquake caused an unprecedented tragedy in the modern history of Mexico, causing 246 deaths and the collapse of 44 buildings (Mayoral et al., 2017). Seismicity can occur within the slab and at greater depths, ~50–300 km (i.e., intermediate-depth (ID) seismicity; Green & Houston, 1995; Yamasaki & Seno, 2003). The origin of ID earthquakes has been hypothesized to be related to the metamorphic dehydration of the subducting oceanic lithosphere as the location of these earthquakes correlates with the depth where dehydration reactions occur within the slab (Yamasaki & Seno, 2003; Hacker et al., 2003; Abers et al., 2013; Ferrand et al., 2017). There are different triggering mechanisms to explain this type of seismicity: (1) dehydration embrittlement (Raleigh & Paterson, 1965; Dobson et al., 2002; Jung & Green, 2004), where embrittlement is connected to the drop in effective confining pressure produced on by the high pore fluid pressure (P_f) during the water released as a result of dehydration, (2) reaction-induced grain size reduction (Green et al., 2015; Incel et al., 2017; Thielmann, 2018), where the creation of nanocrystalline secondary grains and the release of latent heat as a result of the metamorphic reaction are both attributed to the reduction in grain size, which together operate as weakening mechanisms that lead the samples to eventually failure and, (3) dehydration-driven stress transfer (Ferrand et al., 2017) where the aggregates become mechanically unstable as a result of the stress transmission to the surrounding matrix, which results in tensile stress concentrations at the ends of dehydrated antigorite clusters. Another trigger mechanism—which does not necessitate the presence of free fluid—to account for ID seismicity is self-localizing thermal runaway (Ogawa, 1987; Kelemen & Hirth, 2007; John et al., 2009), where localized ductile deformation creates rheological instabilities (Ogawa, 1987; Prieto et al., 2013).

To explain the Puebla-Morelos earthquake, Melgar et al. (2018) proposed that inherited seafloor faults fractures zones were key for governing slab flexure, and thus the bending stresses that caused the rupture of the Cocos plate at the transition between flat to steep subduction. Recently, a model was proposed in which intraslab seismicity was attributed to stresses associated with changes in slab curvature (Sandiford et al., 2019). Although plate-scale stresses and pre-existing zones of weakness are likely important, the potential contribution dehydration reactions to seismicity in the mantle lithosphere of the flat slab portion of the Cocos plate—where the Puebla-Morelos earthquake occurred—has not been investigated for this event. Because pre-existing seafloor faults are sites of increased hydration (due to the water addition to mantle through these structures) and later subduction-related dehydration (Ivandic et al., 2010; Naif et al., 2015; Shillington et al., 2015; Ranero et al., 2003; Prigent et al., 2020), both may act together to cause seismicity.

In this work, we evaluate the metamorphic evolution of the subducted Cocos oceanic lithospheric mantle along the Guerrero segment to investigate the role of mineral dehydration reactions in the nucleation of the Puebla-Morelos 2017 earthquake. We performed thermodynamic petrological modeling assuming local equilibrium at the scale of fault/fracture zones and localized hydrated portions of the upper mantle to quantify the fluid release that might have contributed to trigger intraslab ID seismicity and explore how the mineralogical evolution is influenced by the degree of hydration of pre-existing seafloor faults. We show that along the Mexican flat slab, the reaction brucite + antigorite = olivine + H_2O releases ~185 kg of H_2O per m^3 of subducted hydrated harzburgite. Furthermore, this release of fluid causes an increase of density in the remaining mineral solid assemblage and a significant increase of the system volume ($\Delta V_{r\ solid\ +\ fluid}$) close to the Puebla-Morelos hypocenter. We propose that these likely resulted in increased pore fluid pressures (P_f) and might have triggered fluid-induced fault reactivation—ultimately triggering the Puebla-Morelos 2017 earthquake.

2. Hydration of the lithospheric mantle along seafloor faults

Assessing the effect of hydration along seafloor faults and hydrated portions of the upper mantle is crucial as pre-subduction seafloor hydration and subsequent alteration have been shown to critically control the hydration state of the lithosphere (Hacker, 2008; Hernández-Uribe et al., 2020). Bending faults and oceanic fractures serve as fluid pathways from the seafloor to the uppermost portion of the lithospheric mantle where those faults are spaced ∼2–3 km and can reach depths of ∼20 km beneath the seafloor (e.g., Ranero et al., 2003). Water added to mantle will metasomatize peridotite, generating hydrous serpentinite minerals at < 450 °C (Moody, 1976). Hydration of the upper mantle lithosphere is concentrated along such structures prior to subduction (Ivandic et al., 2010; Naif et al., 2015; Shillington et al., 2015; Ranero et al., 2003; Prigent et al., 2020). Particularly, seafloor faults in the Mexican portion of the Cocos plate, and at the Middle America Trench (MAT), are widespread and common (Ranero et al., 2003; Melgar et al., 2018). Seafloor faults in the Mexican portion have a northwest to southeast trend, which have a mean azimuth of 295° (Melgar et al., 2018).

3. Data and Methods

Here, we investigate the petrological evolution of the hydrated mantle lithosphere along seafloor faults in the subducted Cocos plate along the Guerrero segment of southern Mexico to constraint the potential role of hydrous-mineral breakdown in triggering the Puebla-Morelos earthquake. For this, we forward model the equilibrium phase assemblages (via Gibbs free energy minimization; Connolly, 2009) that would develop along the Guerrero Moho geotherm (the Moho path from Manea & Manea, 2011; Fig. S1) during subduction of three lithologies representative of the oceanic mantle (see below; Table S1), assuming local equilibrium at the scale of fault/fracture zones and localized hydrated portions of the upper mantle.

Phase diagrams were constructed using Perple_X (v. 6.7.3; Connolly, 2009) and the internally consistent thermodynamic data set ds55 (Holland & Powell, 1998; 2004) in the CaO–FeO–MgO–Al_2O_3–SiO_2–H_2O system (Fig. S1). The following activity–composition (a–x) relations for solid solutions were used: antigorite (Padrón-Navarta et al., 2013); clinopyroxene and amphibole (Diener & Powell, 2012), garnet (White et al., 2007); olivine, talc, and epidote (Holland & Powell, 1998); orthopyroxene (Powell & Holland, 1999); chlorite (Holland et al., 1998); plagioclase (Holland & Powell, 2004); spinel (White et al., 2002); and brucite (ideal mixing). Accuracy of assemblage field boundaries on calculated phase diagrams are generally considered to be less than ±0.1 GPa and ±50 °C at the 2σ level (Powell & Holland, 2008), with this variation being largely a function of propagated uncertainty on end-member thermodynamic properties within the data set.

Petrological modeling employed bulk compositions selected from Georoc database (http://georoc.mpch-mainz.gwdg.de/georoc/Start.asp). We selected natural mantle compositions located within the Pacific plate, which we consider representing similar compositions to that of the subducted Cocos lithospheric mantle beneath Mexico (Table S1). We use the harzburgite (sample 125-783A18R-1) from (Parkinson & Pearce, 1998), the lherzolite (sample HK61082601A) from (Kuno, 1969), and the dunite (sample A19) from (Fodor & Galar, 1997) compositions. The original compositions were normalized into the CaO–FeO–MgO–Al_2O_3–SiO_2–H_2O system. The components that are not included (i.e., Na_2O, K_2O, MnO, TiO_2 and Fe_2O_3) in this simplified system are minor in ultramafic systems, making up less than 2 wt. % of the rock's composition (Deschamps et al., 2013). For the first set of models (Figs. 2 and S1), H_2O was considered in excess at the first pressure–temperature (P–T) point of the modeled geotherm. This considers an end-member scenario in which the mantle lithosphere is fully hydrated ("serpentinized") along pre-existing seafloor faults. To explore the effect of different degrees of serpentinization (e.g., incomplete serpentinization along preexisting seafloor faults or further from the sites of maximum hydration along the faults) on the petrophysical properties of the system, we modeled phase equilibria with variable degrees of hydration (net hydration, defined as %H_2O relative to H_2O required for saturation at the starting P–T of the model paths): 80% (~10.88 wt.% H_2O), 60% (~8.16 wt.% H_2O), 40% (~5.44 wt.% H_2O), and 20% (~2.72 wt.% H_2O) for the harzburgite bulk-composition (Fig. 4; Table S2).

4. Results

During early stages of subduction, all modeled compositions are antigorite–brucite serpentinites (Fig. 2) with minor olivine and clinopyroxene; the hydrated lherzolite also stabilizes chlorite due to its higher Al content. There are no significant mineral changes until the slab flattens and the lithosphere isobarically heats. Along the flat slab segment, brucite is fully consumed in each model via the progressive reaction brucite + antigorite = olivine + H_2O ± chlorite (chlorite stabilizes in all except the hydrated harzburgite; Fig. 2). Hydrated harzburgite releases ~8.2 wt. % H_2O, hydrated lherzolite ~3.2 wt. % H_2O, and hydrated dunite ~12.0 wt. % H_2O along this segment (Fig. 3a). The overall dehydration along the flat slab equates to ~185, ~65, and ~336 kg of H_2O per m^3 of subducted hydrated harzburgite, lherzolite, and dunite, respectively. In the hydrated harzburgite and lherzolite, antigorite persists to depths greater than the location of the flat slab, i.e., > 50 km (Fig. 1 & 2). In the modeled hydrated dunite, the reaction antigorite + brucite = olivine + chlorite + H_2O consumes progressively all the brucite and antigorite, where all brucite and antigorite consumes around 500 °C (~ 230 km from the trench). The antigorite breakdown, which is caused by the reaction antigorite = olivine + chlorite + H_2O ± orthopyroxene (Fig. 2), releases ~0.2–2.7 wt.% of H_2O at ~650–700 ºC within ~80–110 km depth (Fig. 3a). At ~80−85 km depth, orthopyroxene stabilizes (except for the hydrated dunite), marking the transition to chlorite hydrated harzburgite/lherzolite assemblages (Fig. 2). Chlorite is the only hydrous mineral remaining after antigorite consumption in the modeled hydrated peridotites. Garnet stabilizes at the expense of chlorite by the following reaction chlorite = garnet + orthopyroxene + H_2O at >147−158 km depth, ~325 km from the trench (Fig. 2).

According to our thermodynamic calculations, the hydrated ultramafic portion of the Cocos slab releases H_2O progressively with major peaks at three depth ranges: ~50 km, ~90−110 km, and ~147−158 km (Figs. 2 & 3). These fluid release pulses are controlled by the antigorite + brucite, antigorite, and chlorite destabilizations, respectively. These dehydration reactions can occur over a range of temperatures; however, due to the limited solid solution of minerals in ultramafic rocks, the maximum peak of fluid released by the reactions occurs over a narrow temperature window (10–20 °C) just before the minerals completely react out of the system (Fig. 3). The release of H_2O by the reaction antigorite + brucite = olivine + H_2O—which is expected to occur along the flat slab segment—results in a distinctly large and positive net ΔV_r of the full system (i.e., $\Delta V_{r\ solid\ +\ fluid}$ = ~0.8%, ~0.3%, and ~1.6% in the hydrated harzburgite, lherzolite, and dunite, respectively; Fig. 3b). The magnitude of ΔV_r is controlled by the amount of brucite that is consumed. The antigorite- and chlorite-out reactions result in a negative net volume change, likely due to the lower volume of H_2O at the higher pressures at which these reactions occur. In all cases, the mineralogical changes result in a significant increase in density of the remaining solid mineral assemblage (Fig. 3c).

4.1 Effects of different hydration degrees along seafloor faults

The results presented above describe an end-member scenario where the inherited seafloor faults served as fluid pathways and fully hydrated the uppermost region of the lithospheric mantle and portions of the seafloor faults itself. In this subsection, we describe the results for other scenarios where only partial hydration (20%, 40%, 60%, and 80%; see Methods) occurs in these regions.

With 20% and 40% of hydration, talc + amphibole and amphibole, respectively, are stable instead of brucite at the flat slab P–T conditions (Fig. 4a, b). Both talc and amphibole are stable to higher pressure in these H_2O-undersaturated models compared to brucite in the H_2O-saturated models; thus, talc- and amphibole-driven dehydration would occur hotter and deeper within the subduction zone (Fig. 4a, b). When talc and amphibole are consumed, the released fluid stabilizes more antigorite rather than producing a large pulse of fluid (Fig. 3d; Fig. 4). Talc and amphibole exhaustion do not produce a significant volume change along the modeled P–T path.

Brucite is stable in all models with >40% hydration (Fig. 5; Fig. 4c, d). Brucite + antigorite dehydration for these models (Fig. 3d), like in the fully hydrated models (Fig. 3a–c), results in a positive volume change (~0.8% and ~1% for 60% and 80% of hydration, respectively; Fig. 3e) and an increase in the density of the remaining solid mineral assemblage (Fig. 3f).

5. Discussion

5.1 The Puebla-Morelos earthquake generating mechanism

Our models indicate that the reaction between brucite and antigorite, with a positive ΔV_r, occurs during flat subduction along the oceanic Moho in the Guerrero subduction zone along pre-existing seafloor faults (Figs. 3–5). The location of where the brucite + antigorite reaction occurs within the Cocos slab match—within uncertainties of the subduction thermal models (±50–100 °C; Peacock, 2009) and petrological models (±50 °C and 0.1 GPa; Powell & Holland, 2008)—the location where the Puebla-Morelos 2017 earthquake nucleated (Fig. 5; Fig. S1). We suggest that fluid released and the increase of volume occurring due to the antigorite + brucite dehydration could have locally increased P_f, reducing the effective normal stress needed to achieve brittle failure (i.e., dehydration embrittlement; Raleigh & Paterson, 1965; Connolly, 1997; Jung & Green, 2004; Peacock, 2001). Therefore, we posit that fluid-induced fault reactivation due to brucite + antigorite dehydration triggered the September 19th Puebla-Morelos earthquake.

Recent observations of reaction-induced porosity within dehydrating serpentinites suggests that mineral dehydration reactions will themselves produce pore space to host fluids (Plümper et al., 2017). Similarly, evidence in the rock record shows the existence of porosity at depths of ~80–90 km in the mafic portion of the slab top (Angiboust & Raimondo, 2022). Further seismic studies observed high V_P/V_S values at mantle depths as well as high b-values (Scholz, 2015) in the Cocos plate (b > 1.5; Rodriguez-Pérez & Zuñiga, 2018) suggest the presence of fluid-filled porosity (Singh & Singh, 2015; Bloch et al., 2018), supporting our proposed model for the Puebla-Morelos earthquake. We argue that the possible accumulation of fluid released along hydrated pre-existing weaknesses over several km depth in the mantle lithosphere (Bloch et al., 2018), and its subsequent channelization (Plümper et al., 2017) could further enhance the seismic potential of the brucite + antigorite reaction at depths where the Puebla-Morelos nucleated. We propose that metamorphically-driven increases in P_f on pre-existing faults provide an excellent triggering mechanism to generate seismicity in a critically stressed environment, something that has been shown in hydrated peridotites in some deformation experiments (Jung et al., 2009; Takahashi et al., 2011).

Other mechanisms that also explain ID earthquakes in subduction zones are dehydration-driven stress transfer (Ferrand et al., 2017) and self-localizing thermal runaways (Keleman & Hirth, 2007; John et al., 2009). Recent studies suggest that these two mechanisms are more viable than the dehydration embrittlement model due to fluid scarcity at mantle depths and because at such depths, dehydration reactions induce a negative net ΔV_r. However, we favor the dehydration embrittlement model to explain the ID Puebla-Morelos earthquake because, as we have described above, fluid was likely present along hydrated seafloor faults, and our calculations indicate a positive ΔV_r induced by the antigorite + brucite dehydration at these depths along these hydrated structures (Fig. 3).

5.2 Hydration of seafloor faults

Our models indicate that brucite assemblages stabilize with >5 wt. % H_2O contents at the *P*–*T* conditions of the upper mantle lithosphere in the Cocos flat slab segment (Figs. 3d−f and 4). Therefore, brucite + antigorite reaction is only likely to occur on pre-existing seafloor faults that are significantly hydrated. Electromagnetic imaging and seismic surveys at outer-rise regions shows that the upper mantle lithosphere is ~20% hydrated on average, and that hydration is not evenly distributed but rather concentrated along faults and/or fractures at the MAT (e.g., Ranero et al., 2003; Ivandic et al., 2010; Naif et al., 2015; Shillington et al., 2015). As a high degree of hydration is needed to stabilize brucite (Figs. 4c & d), we speculate that pre-existing seafloor faults must have served as fluid pathways, being hydrated and hydrating portions of the upper mantle, and thus accounting for different degrees of hydration, brucite stabilization, and the possible nucleation of the Puebla-Morelos earthquake (Figs 3d & f and 4c & d).

Metasomatism may also occur in the pre-existing seafloor faults due to fluid–rock interaction (Allen & Seyfried Jr, 2003; Bach et al., 2004; Boschi et al., 2006). While we only model "unmetasomatized" ultramafic systems, our partial hydrated models show that amphibole + talc bearing assemblages, common in metasomatic horizons, have a higher *P*–*T* stability, therefore it is likely that metasomatism will inhibit brucite stabilization in the flat portion of the Cocos plate.

5.3 Exhumed analogues and evidence in the rock record

As mentioned above, we infer that the brucite + antigorite dehydration reaction promoted the re-activation of an inherited seafloor fault, potentially triggering the Puebla-Morelos earthquake. We envision than an excellent analogue in the rock record for our proposed model are the dunites of the Leka Ophiolite in the central Norwegian Caledonides, which show evidence of localized hydration, and subsequence dehydration + faulting along discrete faults (Dunkel et al., 2017).

The progressive dehydration of the brucite + antigorite reaction predicted by our models is further comparable to other modeling estimates in the literature (e.g., Padrón-Navarta et al., 2013) and with microtextural observations of the brucite + antigorite reaction in the rock record for similar subduction-related lithologies. For example, brucite veins crosscutting olivine and the formation of olivine with a coarse grain size and rich in magnetite inclusions suggesting fluid release (Hermann et al., 2000; Kempf et al., 2020).

5. Conclusions

Our findings highlight the importance of brucite breakdown for promoting important petrophysical changes in the Moho and hydrated portions of the mantle, and potentially on triggering earthquakes. The brucite + antigorite dehydration reaction could also account for other ID earthquakes close to the Puebla-Morelos area with similar focal mechanisms, depths, and magnitudes (Singh et al., 1999), and in subduction zones worldwide with similar thermal structures (e.g., Cascadia, Parsons et al., 1998; NW Colombia, Gutscher et al., 2000, Alaska, Brocher et al., 1994).

Particularly, we find that the reaction brucite + antigorite = olivine + H_2O results in substantial dehydration and significant volume and density increase at ~50‒60 km depth in the subducted Cocos Moho, where the Puebla-Morelos earthquake nucleated. We propose that this reaction induced fault reactivation, triggering the Puebla-Morelos earthquake. Our model results show that this reaction only occurs in strongly hydrated portions of the uppermost lithospheric mantle, such as in pre-existing seafloor faults (e.g., bending faults, oceanic fractures zones, and spreading faults), and highlights the importance of subducting seafloor faults for ID seismicity worldwide.

Acknowledgements

We thank V. Manea for providing the thermal models for the calculations. D. Melgar and J. Tago are thanked for helpful discussions about the Puebla-Morelos earthquake. J. Warren and two anonymous reviewers are thanked for their helpful and thoughtful comments. Q. Williams is thanked for editorial handling. J. Hermann, T. John, and T. Ferrand are thanked for their positive comments that improved earlier versions of this work.

Data availability statement

The whole-rock data used for the petrological modeling as well as the modeling results from this paper can be found in the Mendeley database (DOI:10.17632/4pbnmxbgcd.4): (https://data.mendeley.com/datasets/4pbnmxbgcd/4)

REFERENCES

1. Allen, D. E., & Seyfried Jr, W. E. (2003). Compositional controls on vent fluids from ultramafic-hosted hydrothermal systems at mid-ocean ridges: An experimental study at 400 C, 500 bars. Geochimica et Cosmochimica Acta, 67(8), 1531-1542.
2. Angiboust, S., & Raimondo, T. (2022). Permeability of subducted oceanic crust revealed by eclogite-facies vugs. Geology, 50, 964-968.
3. Abers, G. A., Nakajima, J., van Keken, P. E., Kita, S., & Hacker, B. R. (2013). Thermal–petrological controls on the location of earthquakes within subducting plates. Earth and Planetary Science Letters, 369, 178-187.
4. Bach, W., Garrido, C. J., Paulick, H., Harvey, J., & Rosner, M. (2004). Seawater- peridotite interactions: First insights from ODP Leg 209, MAR 15 N. Geochemistry, Geophysics, Geosystems, 5(9), Q09F26.
5. Bloch, W., John, T., Kummerow, J., Salazar, P., Krüger, O. S., & Shapiro, S. A. (2018). Watching dehydration: Seismic indication for transient fluid pathways in the oceanic mantle of the subducting Nazca slab. Geochemistry, Geophysics, Geosystems, 19(9), 3189-3207.

6. Boschi, C., Früh- Green, G. L., Delacour, A., Karson, J. A., & Kelley, D. S. (2006). Mass transfer and fluid flow during detachment faulting and development of an oceanic core complex, Atlantis Massif (MAR 30 N). Geochemistry, Geophysics, Geosystems, 7(1), Q01004.
7. Connolly, J. A. D. (1997). Devolatilization- generated fluid pressure and deformation-propagated fluid flow during prograde regional metamorphism. Journal of Geophysical Research: Solid Earth, 102(B8), 18149-18173.
8. Connolly, J. A. D. (2009). The geodynamic equation of state: what and how. Geochemistry, Geophysics, Geosystems, 10(10), Q10014.
9. Cruz-Atienza, V. M., Tago, J., Villafuerte, C., Wei, M., Garza-Girón, R., Dominguez, L. A., et al. (2021). Short-term interaction between silent and devastating earthquakes in Mexico. Nature Communications, 12, 2171.
10. Deschamps, F., Godar, M., Guillot, S., & Hattori, K. (2013). Geochemistry of subduction zone serpentinites: A review. Lithos, 178, 96-127.
11. Diener, J. F. A., & Powell, R. (2012). Revised activity-composition models for clinopyroxene and amphibole. Journal of Metamorphic Geology, 30, 131–142.
12. Dobson, D. P., Meredith, P. G., & Boon, S. A. (2002). Simulation of subduction zone seismicity by dehydration of serpentine. Science, 298(5597), 1407-1410.
13. Dunkel, K. G., Austrheim, H., Renard, F., Cordonnier, B., & Jamtveit, B. (2017). Localized slip controlled by dehydration embrittlement of partly serpentinized dunites, Leka Ophiolite Complex, Norway. Earth and Planetary Science Letters, 463, 277–285.

14. Ferrand, T. P., Hilairet, N., Incel, S., Deldicque, D., Labrousse, L., Gasc, J., et al. (2017). Dehydration-driven stress transfer triggers intermediate-depth earthquakes. Nature Communication, 8, 15247.

15. Fodor, R. V., & Galar, P. A (1997). View into the subsurface of Mauna Kea volcano, Hawaii: crystallization processes interpreted through the petrology and petrography of gabbroic and ultramafic xenoliths. Journal of Petrology, 38(5), 581−624.

16. Green, H. W., & Houston, H. (1995). The Mechanics of Deep Earthquakes. Annual Review of Earth and Planetary Sciences, 23, 169–213.

17. Green II, H. W., Shi, F., Bozhilov, K., Xia, G., & Reches, A. Z. (2015). Phase transformation and nanometric flow cause extreme weakening during fault slip. Nature Geoscience, 8(6), 484-489.

18. Gutscher, M. A., Spakman, W., Bijwaard, H., & Engdahl, E. R. (2000). Geodynamics of flat subduction: Seismicity and tomographic constraints from the Andean margin. Tectonics, 19(5), 814-833.

19. Hacker, B. R. (2008). H_2O subduction beyond arcs. Geochemistry, Geophysics, Geosystems, 9(3).

20. Hacker, B. R., Peacock, S. M., Abers, G. A., & Holloway, S. D. (2003). Subduction factory 2. Are intermediate-depth earthquakes in subducting slabs linked to metamorphic dehydration reactions? Journal of Geophysics Research: Solid Earth, 108, 203.

21. Hermann, J., Müntener, O., & Scambelluri, M. (2000). The importance of serpentinite mylonites for subduction and exhumation of oceanic crust. Tectonophysics, 327, 225−238.

22. Hernández-Uribe, D., Palin, R. M., Cone, K. A., & Cao, W. (2020). Petrological implications of seafloor hydrothermal alteration of subducted mid-ocean ridge basalt. Journal of Petrology, 61(9), egaa086.

23. Holland T. J. B., Baker J., & Powell R. (1998). Mixing properties and activity-composition relationships of chlorites in the system MgO-FeO-Al2O3-SiO2-H2O. European Journal of Mineralogy, 10, 395−406.

24. Holland, T. J. B., & Powell, R. (1998). An internally consistent thermodynamic data set for phases of petrological interest. Journal of Metamorphic Geology, 16, 309–343.

25. Holland, T. J. B., & Powell, R. (2004). Activity–composition relations for phases in petrological calculations: an asymmetric multicomponent formulation. Contributions to Mineralogy and Petrology, 145(4), 492–501.

26. Incel, S., Hilairet, N., Labrousse, L., John, T., Deldicque, D., Ferrand, T. P., et al. (2017). Laboratory earthquakes triggered during eclogitization of lawsonite-bearing blueschist. Earth & Planetary Science Letters, 459, 320-331.

27. Ivandic, M., Grevemeyer, I., Bialas, J., & Petersen, C. J. (2010). Serpentinization in the trench-outer rise region offshore of Nicaragua: constraints from seismic refraction and wide-angle data. Geophysical Journal International, 180, 1253–1264.

28. John, T., Medvedev, S., Rüpke, L. H., Andersen, T. B., Podladchikov, Y. Y., & Austrheim, H. (2009). Generation of intermediate-depth earthquakes by self-localizing thermal runaway. Nature Geoscience, 2(2), 137-140.

29. Jung, H., & Green, H. W. (2004). Experimental faulting of serpentinite during dehydration: Implications for earthquakes, seismic low-velocity zones, and anomalous hypocenter distributions in subduction zones. International Geology Review, 46(12), 1089-1102.

30. Jung, H., Fei, Y., Silver, P. G., & Green II, H. W. (2009). Frictional sliding in serpentine at very high pressure. Earth and Planetary Science Letters, 277(1-2), 273-279.

31. Kelemen, P. B., & Hirth, G. (2007). A periodic shear-heating mechanism for intermediate-depth earthquakes in the mantle. Nature, 446(7137), 787-790.

32. Kempf, E. D., Hermann, J., Reusser, E., Baumgartner, L. P., & Lanari, P. (2020). The role of the antigorite plus brucite to olivine reaction in subducted serpentinites (Zermatt, Switzerland). Swiss Journal of Geosciences, 113, 16.
33. Kuno, H. (1969). Mafic and ultramafic nodules in basaltic rocks of Hawaii. Geological Society of America Memory, 115, 189−234.
34. Manea, V. C., & Manea, M. (2011). Flat-Slab Thermal Structure and Evolution Beneath Central Mexico. Pure and Applied Geophysics, 168, 1475–1487.
35. Mayoral, J. M., Hutchinson, T. C., & Franke, K. W. (2017). Geotechnical engineering reconnaissance of the 19 September 2017 Mw 7.1 Puebla-Mexico City earthquake, GEER association report no. GEER-055A.
36. Melgar, D., Pérez-Campos, X., Ramirez-Guzman, L., Spica, Z., Espíndola, V.H., Hammond, W.C., et al. (2018). Bend Faulting at the Edge of a Flat Slab: The 2017 Mw 7.1 Puebla-Morelos, Mexico Earthquake. Geophysical Research Letters, 45, 2633–2641.
37. Mirwald, A., Cruz- Atienza, V. M., Díaz- Mojica, J., Iglesias, A., Singh, S. K., Villafuerte, C., & Tago, J. (2019). The 19 September 2017 (M w 7.1) intermediate- depth Mexican earthquake: A slow and energetically inefficient deadly shock. Geophysical Research Letters, 46(4), 2054-2064.
38. Moody, J. B. (1976). Serpentinization: a review. Lithos, 9(2), 125-138.
39. Müller, R. D., Sdrolias, M., Gaina, C., & Roest, W. R. (2008). Age, spreading rates, and spreading asymmetry of the world's ocean crust. Geochemistry, Geophysics, Geosystems, 9(4).
40. Naif, S., Key, K., Constable, S., & Evans, R. L. (2015). Water-rich bending faults at the Middle America Trench. Geochemistry, Geophysics, Geosystems, 16, 2582–2597.

41. Ogawa, M. (1987). Shear instability in a viscoelastic material as the cause of deep focus earthquakes. Journal of Geophysical Research: Solid Earth, 92(B13), 13801-13810.

42. .

43. Padrón-Navarta, J. A., Sánchez-Vizcaíno, V. L., Hermann, J., Connolly, J. A., Garrido, C. J., Gómez-Pugnaire, M. T., et al. (2013). Tschermak"s substitution in antigorite and consequences for phase relations and water liberation in high-grade serpentinites. Lithos, 178, 186−196.

44. Parkinson, I. J., & Pearce, J. A. (1998). Peridotites from the Izu–Bonin–Mariana forearc (ODP Leg 125): evidence for mantle melting and melt–mantle interaction in a supra-subduction zone setting. Journal of Petrology, 39(9), 1577−1618.

45. Parsons, T., Trehu, A. M., Luetgert, J. H., Miller, K., Kilbride, F., Wells, R. E., ... & Christensen, N. I. (1998). A new view into the Cascadia subduction zone and volcanic arc: Implications for earthquake hazards along the Washington margin. Geology, 26(3), 199-202.

46. Peacock, S. M. (2001). Are the lower planes of double seismic zones caused by serpentine dehydration in subducting oceanic mantle? Geology, 29, 299-302.

47. Peacock, S. M. (2009). Thermal and metamorphic environment of subduction zone episodic tremor and slip. Journal of Geophysical Research: Solid Earth, 114, B00A07.

48. Pérez-Campos, X., Kim, Y., Husker, A., Davis, P. M., Clayton, R. W., Iglesias, A., et al. (2008). Horizontal subduction and truncation of the Cocos Plate beneath central Mexico. Geophysical Research Letters, 35, L18303.

49. Plümper, O., John, T., Podladchikov, Y. Y., Vrijmoed, J. C., & Scambelluri, M. (2017). Fluid escape from subduction zones controlled by channel-forming reactive porosity. Nature Geoscience, 10, 150−156.

50. Powell, R., & Holland, T. J. B. (1999). Relating formulations of the thermodynamics of mineral solid solutions; activity modeling of pyroxenes, amphiboles, and micas. American Mineralogy, 84, 1–14.

51. Powell, R., & Holland, T. J. B. (2008). On thermobarometry. Journal of Metamorphic Geology, 26, 155–179.

52. Prieto, G. A., Florez, M., Barrett, S. A., Beroza, G. C., Pedraza, P., Blanco, J. F., et al. (2013). Seismic evidence for thermal runaway during intermediate- depth earthquake rupture. Geophysical Research Letters, 40(23), 6064-6068.

53. Prigent, C., Warren, J. M., Kohli, A. H. & Teyssier, C. 2020. Fracture-mediated deep seawater flow and mantle hydration on oceanic transform faults. Earth & Planetary Science Letters 532, 115988.

54. Raleigh, C. B., & Paterson, M. S. (1965). Experimental deformation of serpentinite and its tectonic implications. Journal of Geophysical Research, 70(16), 3965-3985.

55. Ranero, C. R., Phipps Morgan, J., McIntosh, K., & Reichert, C. (2003). Bending-related faulting and mantle serpentinization at the Middle America trench. Nature, 425, 367–373.

56. Rodríguez-Pérez, Q., & Zuñiga, F. R. (2018). Imaging b-value depth variations within the Cocos and Rivera plates at the Mexican subduction zone. Tectonophysics, 734, 33-43.

57. Sandiford, D., Moresi, L., Sandiford, M., & Yang, T. (2019). Geometric controls on flat slab seismicity. Earth and Planetary Science Letters, 527, 115787.

58. Scholz, C. H. (2015). On the stress dependence of the earthquake b value. Geophysical Research Letters, 42(5), 1399-1402.

59. Shillington, D. J., Bécel, A., Nedimović, M. R., Kuehn, H., Webb, S. C., Abers, G. A., et al. (2015). Link between plate fabric, hydration and subduction zone seismicity in Alaska. Nature Geoscience, 8, 961–964.

60. Singh, C., & Singh, S. (2015). Imaging b- value variation beneath the Pamir–Hindu Kush region. Bulletin of the Seismological Society of America, 105(2A), 808-815.
61. Singh, S. K., Ordaz, M., Pacheco, J. F., Quaas, R., Alcantara, L., Alcocer, S., et al. (1999). A preliminary report on the Tehuacan, Mexico earthquake of June 15, 1999 (Mw= 7.0). Seismological Research Letters, 70, 489−504.
62. Takahashi, M., Uehara, S. I., Mizoguchi, K., Shimizu, I., Okazaki, K., & Masuda, K. (2011). On the transient response of serpentine (antigorite) gouge to stepwise changes in slip velocity under high- temperature conditions. Journal of Geophysical Research: Solid Earth, 116, B10405.
63. Thielmann, M. (2018). Grain size assisted thermal runaway as a nucleation mechanism for continental mantle earthquakes: Impact of complex rheologies. Tectonophysics, 746, 611-623.
64. SSN (2020). Servicio Sismológico Nacional, Instituto de Geofísica, Universidad Nacional Autónoma de México. Retrieved from: https://ssn.unam.mx. Doi:doi.org/10.21766/SSNMX/EC/MX (2017).
65. White, R. W., Powell, R., & Clarke, G. L. (2002). The interpretation of reaction textures in Fe-rich metapelitic granulites of the Musgrave Block, Central Australia: Constraints from mineral equilibria calculations in the system. Journal of Metamorphic Geology, 20, 41–55.
66. White, R. W., Powell, R., & Holland, T. J. B. (2007). Progress relating to calculation of partial melting equilibria for metapelites. Journal of Metamorphic Geology, 25, 511–527.
67. Yamasaki, T., & Seno, T. (2003). Double seismic zone and dehydration embrittlement of the subducting slab. Journal of Geophysics Research: Solid Earth, 108, 2212.

68. Kelemen, P. B., & Hirth, G. (2007). A periodic shear-heating mechanism for intermediate-depth earthquakes in the mantle. Nature, 446(7137), 787-790.

69. Brocher, T. M., Fuis, G. S., Fisher, M. A., Plafker, G., Moses, M. J., Taber, J. J., & Christensen, N. I. (1994). Mapping the megathrust beneath the northern Gulf of Alaska using wide-angle seismic data. Journal of Geophysical Research: Solid Earth, 99(B6), 11663-11685

FIGURES CAPTIONS

Figure 1. Seismicity in central Mexico. (a) The thick orange line doubled with dashed back line indicates the profile location of the thermal model of Manea & Manea (2011). Black dashed lines are depth isolines (km) of the Cocos plate beneath the North American plate. Black lines indicate the distribution of seafloor fabric. Purple, yellow, and blue shaded areas show zones of ID earthquakes, thrust earthquakes, and recent slow slip events (SSE), respectively (modified after Mirwald et al., 2019; Cruz-Atienza et al., 2021). (b) Thermal model (Manea & Manea, 2011) and seismic features (SSN, 2020) in western and central Mexico. White circles show the hypocenter of earthquakes (< 70 km depth) that occurred within the Cocos plate during 2017–2020.

Figure 2. Equilibrium mineral assemblages along the Guerrero geotherm. (a–c) Mineral proportions for hydrated harzburgite, lherzolite, and dunite, respectively. Brucite is completely consumed regardless of the modeled composition at 480–500 ºC and ~1.5 GPa along the flat slab segment. The gentle slope, flat slab, and steep slope refer to the areas of the slab as shown in Figure 1. Brc–brucite; Atg–antigorite; Ol–olivine; Opx–orthopyroxene; Cpx–clinopyroxene; Grt–garnet; Chl–chlorite.

Figure 3. Petrophysical properties of the subducted oceanic Cocos plate. (a) H_2O released, (b) ΔV_r (solids + fluid), and (c) density of solids evolution during subduction of the hydrated ultramafic portion of the Cocos oceanic lithospheric mantle. (d–e) Effects of different degrees of hydration (of a harzburgite) on (d) H_2O released, (e) ΔV_r (solids + fluid), and (f) density.

Figure 4. The effect of different degrees of hydration for harzburgite during subduction. Calculated mineral assemblages along the Guerrero geotherm at (a) 20%, (b) 40%, (c) 60%, and (d) 80% of hydration.

Figure 5. Thermal model and location of the dehydration reactions of the subducted oceanic Cocos plate. (a) Thermal model for central Mexico (Manea & Manea, 2011) showing the location and focal mechanism of the 2017 Puebla-Morelos earthquake, and the position of brucite, antigorite, and chlorite dewatering (at Moho depths). (b) Summarized *P*–*T* diagram for a hydrated harzburgite with the stability of brucite and antigorite, and the *P*–*T* path with its uncertainties of ±75 °C (the gray shaded areas; see also Fig. S1).

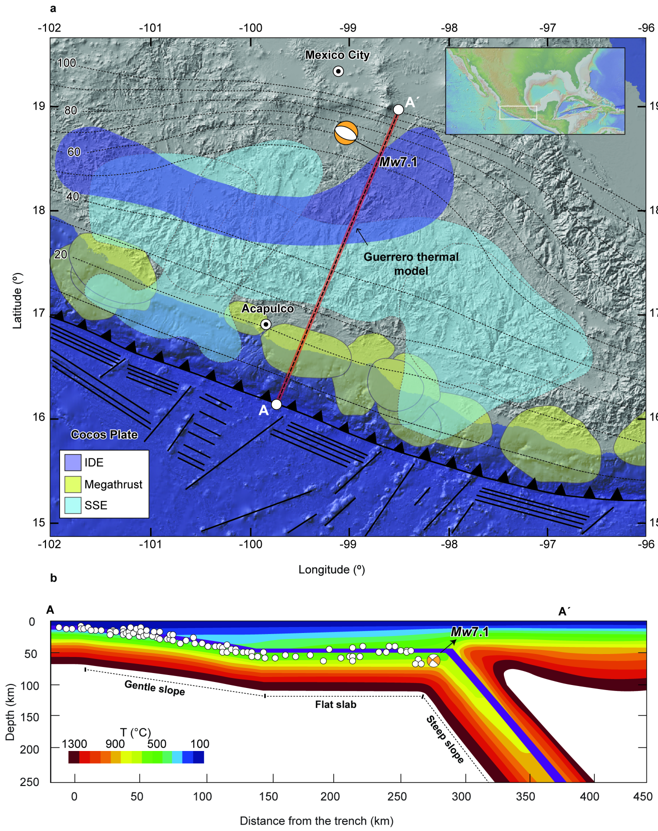
a
-102
-101
-100
-99
-98
-97
-96
19
18
17
16
15
Latitude (°)
Longitude (°)
Mexico City
A´
Mw7.1
Guerrero thermal model
Acapulco
A
Cocos Plate
IDE
Megathrust
SSE
100
80
60
40
20
b
A
A´
Mw7.1
Gentle slope
Flat slab
Steep slope
Depth (km)
T (°C)
1300
900
500
100
0
50
100
150
200
250
300
350
400
450
Distance from the trench (km)

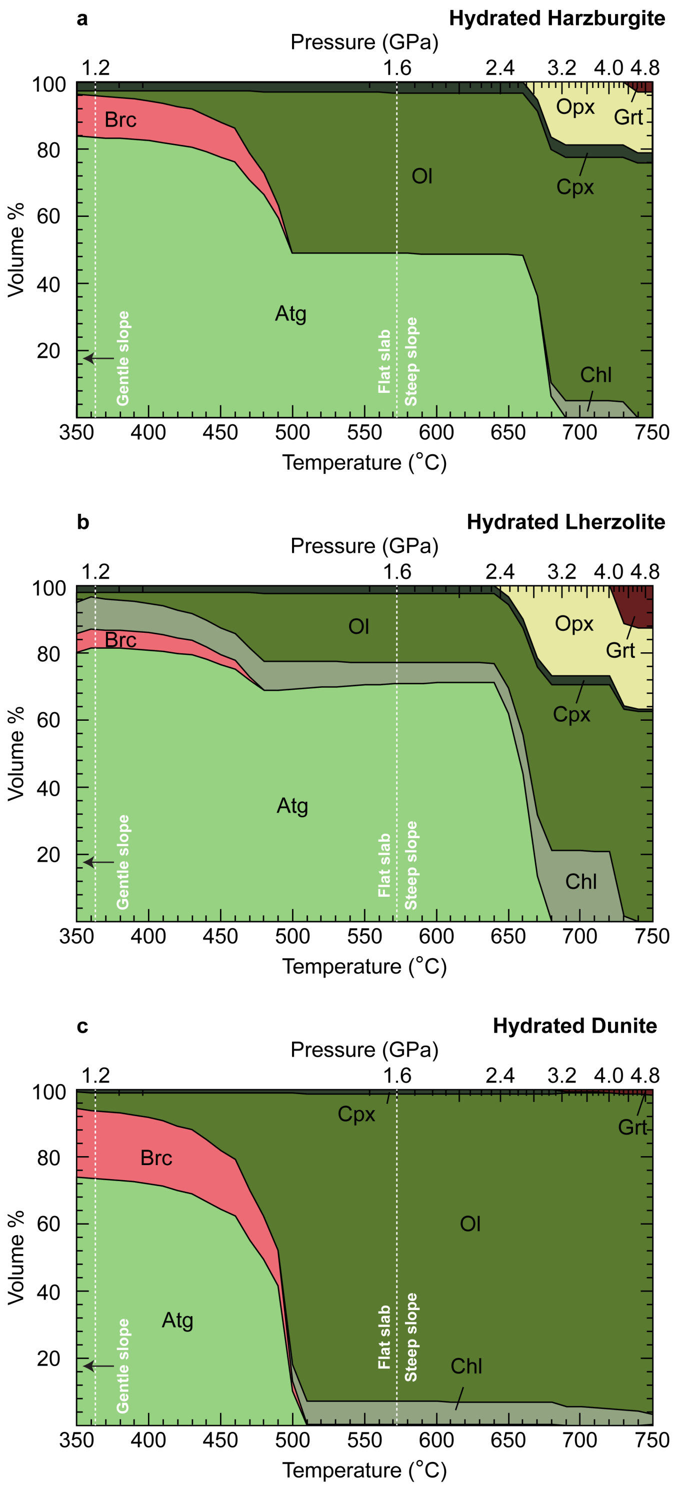
a
Hydrated Harzburgite
Pressure (GPa)
1.2
1.6
2.4
3.2
4.0
4.8
100
80
60
40
20
Volume %
Brc
Ol
Opx
Grt
Cpx
Atg
Chl
Gentle slope
Flat slab
Steep slope
350
400
450
500
550
600
650
700
750
Temperature (°C)
b
Hydrated Lherzolite
Pressure (GPa)
1.2
1.6
2.4
3.2
4.0
4.8
100
80
60
40
20
Volume %
Brc
Ol
Opx
Grt
Cpx
Atg
Chl
Gentle slope
Flat slab
Steep slope
350
400
450
500
550
600
650
700
750
Temperature (°C)
c
Hydrated Dunite
Pressure (GPa)
1.2
1.6
2.4
3.2
4.0
4.8
100
80
60
40
20
Volume %
Cpx
Grt
Brc
Ol
Atg
Chl
Gentle slope
Flat slab
Steep slope
350
400
450
500
550
600
650
700
750
Temperature (°C)

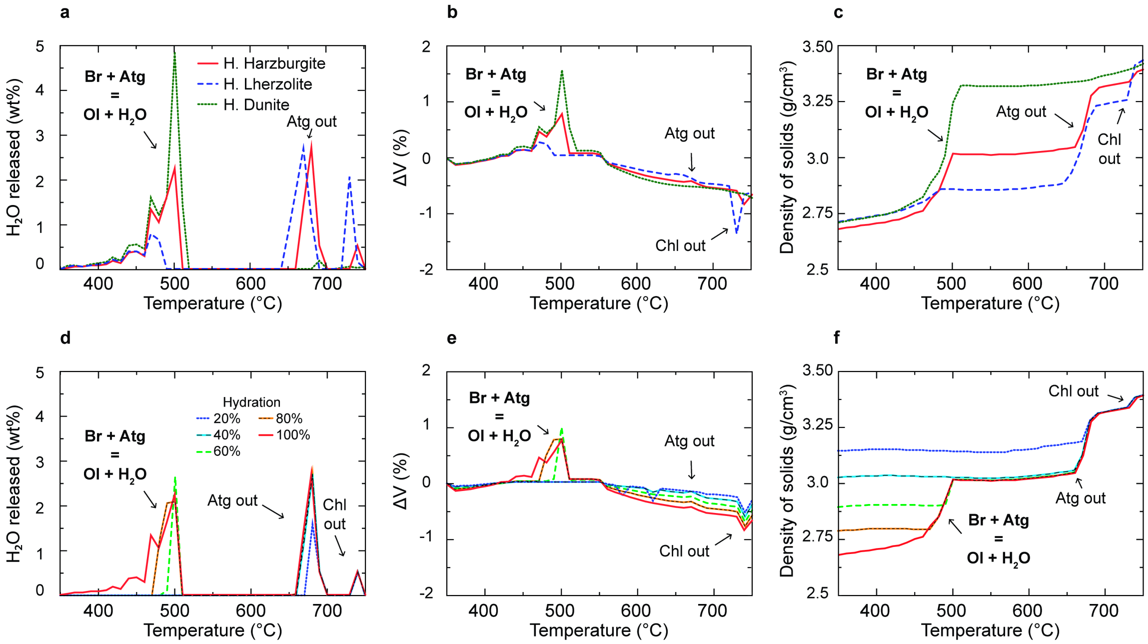
a
b
c
d
e
f
Br + Atg
=
Ol + H_2O
H. Harzburgite
H. Lherzolite
H. Dunite
Atg out
Chl out
Hydration
20%
40%
60%
80%
100%
H_2O released (wt%)
ΔV (%)
Density of solids (g/cm³)
Temperature (°C)

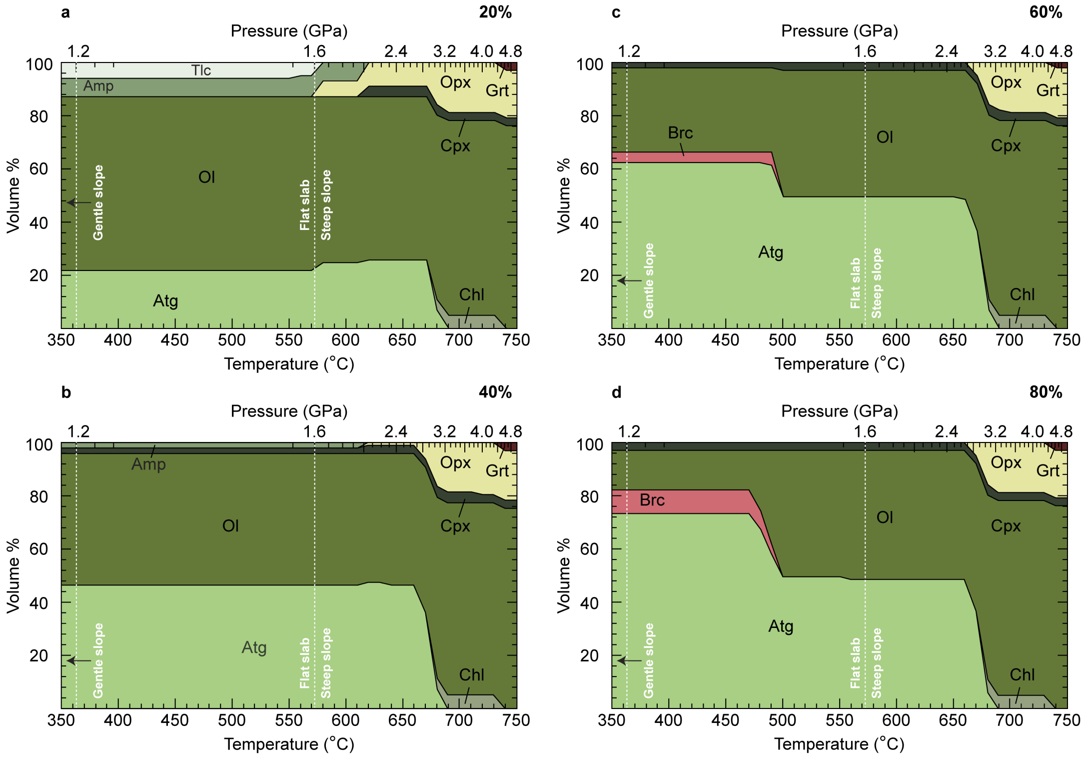
a
20%
Pressure (GPa)
1.2
1.6
2.4
3.2
4.0
4.8
Tlc
Amp
Opx
Grt
Ol
Cpx
Atg
Chl
Gentle slope
Flat slab
Steep slope
Volume %
Temperature (°C)
b
40%
Amp
Ol
Opx
Grt
Cpx
Atg
Chl
c
60%
Brc
Ol
Opx
Grt
Cpx
Atg
Chl
d
80%
Brc
Ol
Opx
Grt
Cpx
Atg
Chl

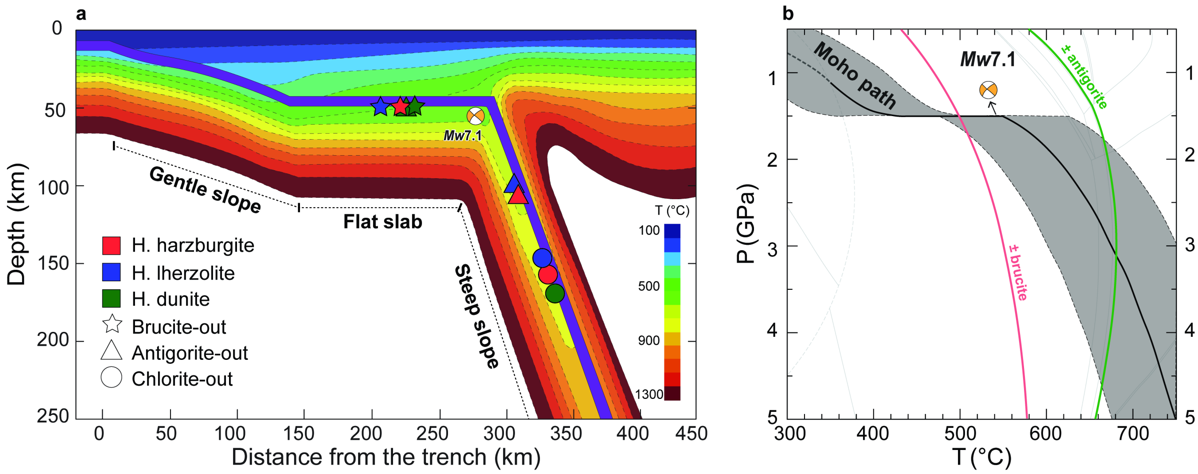
a
Depth (km)
Distance from the trench (km)
Gentle slope
Flat slab
Steep slope
Mw7.1
H. harzburgite
H. lherzolite
H. dunite
Brucite-out
Antigorite-out
Chlorite-out
T (°C)
b
Moho path
Mw7.1
± antigorite
± brucite
P (GPa)
T (°C)